

Actin-Depolymerizing Factor2-Mediated Actin Dynamics Are Essential for Root-Knot Nematode Infection of *Arabidopsis*

Mathilde Clément,^{a,1,2} Tijs Ketelaar,^{b,c,2} Natalia Rodiuc,^{a,2} Mohamed Youssef Banora,^a Andrei Smertenko,^c Gilbert Engler,^a Pierre Abad,^a Patrick J. Hussey,^c and Janice de Almeida Engler^{a,3}

^aUnité Mixte de Recherches Interactions Biotiques et Santé Végétale, Institut National de la Recherche Agronomique, Centre National de la Recherche Scientifique, Université de Nice-Sophia Antipolis, F-06903 Sophia Antipolis, France

^bLaboratory of Plant Cell Biology, Wageningen University, 6703 BD Wageningen, The Netherlands

^cSchool of Biological and Biomedical Sciences, University of Durham, Durham DH1 3LE, United Kingdom

Reorganization of the actin and microtubule networks is known to occur in targeted vascular parenchymal root cells upon infection with the nematode *Meloidogyne incognita*. Here, we show that actin-depolymerizing factor (ADF) is upregulated in the giant feeding cells of *Arabidopsis thaliana* that develop upon nematode infection and that knockdown of a specific ADF isotype inhibits nematode proliferation. Analysis of the levels of transcript and the localization of seven ADF genes shows that five are upregulated in galls that result from the infection and that ADF2 expression is particularly increased between 14 and 21 d after nematode inoculation. Further analysis of ADF2 function in inducible RNA interference lines designed to knock down ADF2 expression reveals that this protein is required for normal cell growth and plant development. The net effect of decreased levels of ADF2 is F-actin stabilization in cells, resulting from decreased F-actin turnover. In nematode-infected plants with reduced levels of ADF2, the galls containing the giant feeding cells and growing nematodes do not develop due to the arrest in growth of the giant multinucleate feeding cells, which in turn is due to an aberrant actin network.

INTRODUCTION

The plant actin cytoskeleton undertakes a striking reorganization in response to internal and external signals and is involved in different cellular processes essential for plant development. These processes include cell division, differentiation and expansion, regulation of cell polarity, cytoplasmic streaming, organelle movement and rearrangement, cell-to-cell communication through plasmodesmata, and response to wounding, pathogen attack, and hormone distribution (reviewed in Kost et al., 1999; Volkmann and Baluska, 1999; Staiger, 2000; Wasteneys and Galway, 2003; Hussey et al., 2006; Staiger and Blanchoin, 2006). In response to these multiple cellular activities, the actin cytoskeleton is dynamically reorganized and remodeled by a range of actin binding proteins (ABPs) (Ayscough, 1998; Hussey et al., 2006). Members of the actin-depolymerizing factor (ADF) or cofilin family are key regulators of the turnover of filamentous

actin (Staiger et al., 1997; Carlier, 1998; Maciver and Hussey, 2002). The ADF/cofilin family proteins bind G- and F-actin and increase actin turnover by severing actin filaments and by increasing the rate of dissociation of actin monomer from the pointed ends (Carlier et al., 1997; Maciver, 1998; Chen et al., 2000; Andrianantoandro and Pollard, 2006; Pavlov et al., 2007). ADF/cofilin activity in plants is regulated by reversible phosphorylation, specific phosphoinositides, and pH (Smertenko et al., 1998; Allwood et al., 2002).


The *Arabidopsis thaliana* ADF gene family consists of 11 expressed members that group phylogenetically into four ancient subclasses (Rhee et al., 2003; Feng et al., 2006). The expression patterns of various plant ADFs from *Zea mays*, *Lilium longiflorum*, and *Nicotiana tabacum* resulted in the classification of vegetative- and pollen-specific types (Kim et al., 1993; Lopez et al., 1996; Jiang et al., 1997; Allwood et al., 2002; Chen et al., 2002). These data support the previously proposed model that differentially expressed actins and ABPs coevolved in particular organs, tissues, and cells (Meagher et al., 1999). Fusions of promoters of some ADF genes with a β -glucuronidase (GUS) reporter revealed that *Arabidopsis ADF1* and *ADF6* are expressed in the vascular tissues of all organs, whereas expression of *ADF5* is restricted to the root apical meristem (Dong et al., 2001b). Recently, Ruzicka et al. (2007) characterized the tissue-specific and developmental expression of all *Arabidopsis* ADF genes and the subcellular localization of several protein isoforms. It has been demonstrated that subclass I ADFs (*ADF1*, *ADF2*, *ADF3*, and *ADF4*) are strongly and constitutively expressed in all vegetative and reproductive tissues except pollen. Subclass II genes (*ADF7*, *ADF8*, *ADF10*, and *ADF11*) are particularly expressed in mature pollen and pollen tubes or root hair-forming

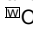
¹ Current address: Laboratory of Plant Development Biology, Unité Mixte de Recherche 6191, Centre National de la Recherche Scientifique/Commissariat à l'Energie Atomique/Université Aix-Marseille, Service de Biologie Végétale et de Microbiologie Environnementale/Institut de Biologie Environnementale et Biotechnologie Commissariat à l'Energie Atomique, F-13108 Cadarache St. Paul lez Durance, France.

² These authors contributed equally to this work.

³ Address correspondence to janice.almeida-engler@sophia.inra.fr.

The author responsible for distribution of materials integral to the findings presented in this article in accordance with the policy described in the Instructions for Authors (www.plantcell.org) is: Janice de Almeida Engler (janice.almeida-engler@sophia.inra.fr).

 Some figures in this article are displayed in color online but in black and white in the print edition.

 Online version contains Web-only data.

www.plantcell.org/cgi/doi/10.1105/tpc.109.069104

epidermal cells. Members of subclass III (*ADF5* and *ADF9*) are weakly expressed in vegetative tissues but upregulated in growing and/or differentiating cells, including callus, emerging leaves, and meristem. The subclass IV gene (*ADF6*) is constitutively expressed at moderate levels in all tissues, including pollen. Immunocytochemical analysis with subclass-specific antibodies have shown that subclass I isotypes localize to both the cytoplasm and the nucleus of leaf cells, while subclass II isotypes localize predominantly to the cytoplasm at the tip region of elongating root hairs and pollen tubes (Ruzicka et al., 2007).

Rearrangement of microfilaments and microtubules can be induced in the parenchymal target cells of the vascular cylinder upon infection by sedentary phytoparasitic nematodes (de Almeida Engler et al., 2004). Parasitic nematodes are major plant pests attacking a wide host range resulting in significant world crop loss (Fuller et al., 2008). They present a rather complex life cycle. In a compatible host, which includes *Arabidopsis* (Sijmons et al., 1991), second-stage juveniles (J2) penetrate the plant root and migrate into the vascular cylinder. Giant feeding cells in-

duced by the root-knot nematode *Meloidogyne incognita* start by expansion of parenchyma cells in the root vascular tissue. These developing giant cells hold a dense cytoplasm filled with organelles and undergo rounds of synchronous nuclear division uncoupled from cytokinesis, during which each nucleus becomes highly polyploid (Bird and Kaloshian, 2003). A functional mitotic apparatus containing multiple large and malformed spindles and often misoriented and aborted phragmoplasts is present throughout the numerous mitotic events observed in giant cells (de Almeida Engler et al., 2004, 2005). Nematode infection can induce permanent rearrangements of the actin cytoskeleton. During giant cell expansion, the organization of the actin cytoskeleton is significantly altered, showing large numbers of thick actin bundles and cables throughout the cell cortex. On the other hand, cytoplasmic actin bundles are shorter, thinner, and distributed at random within a slightly amorphous actin staining most likely resulting from monomers and/or broken down filaments (de Almeida Engler et al., 2004). Giant cells function as carbon sinks and have been described as transfer cells (Jones

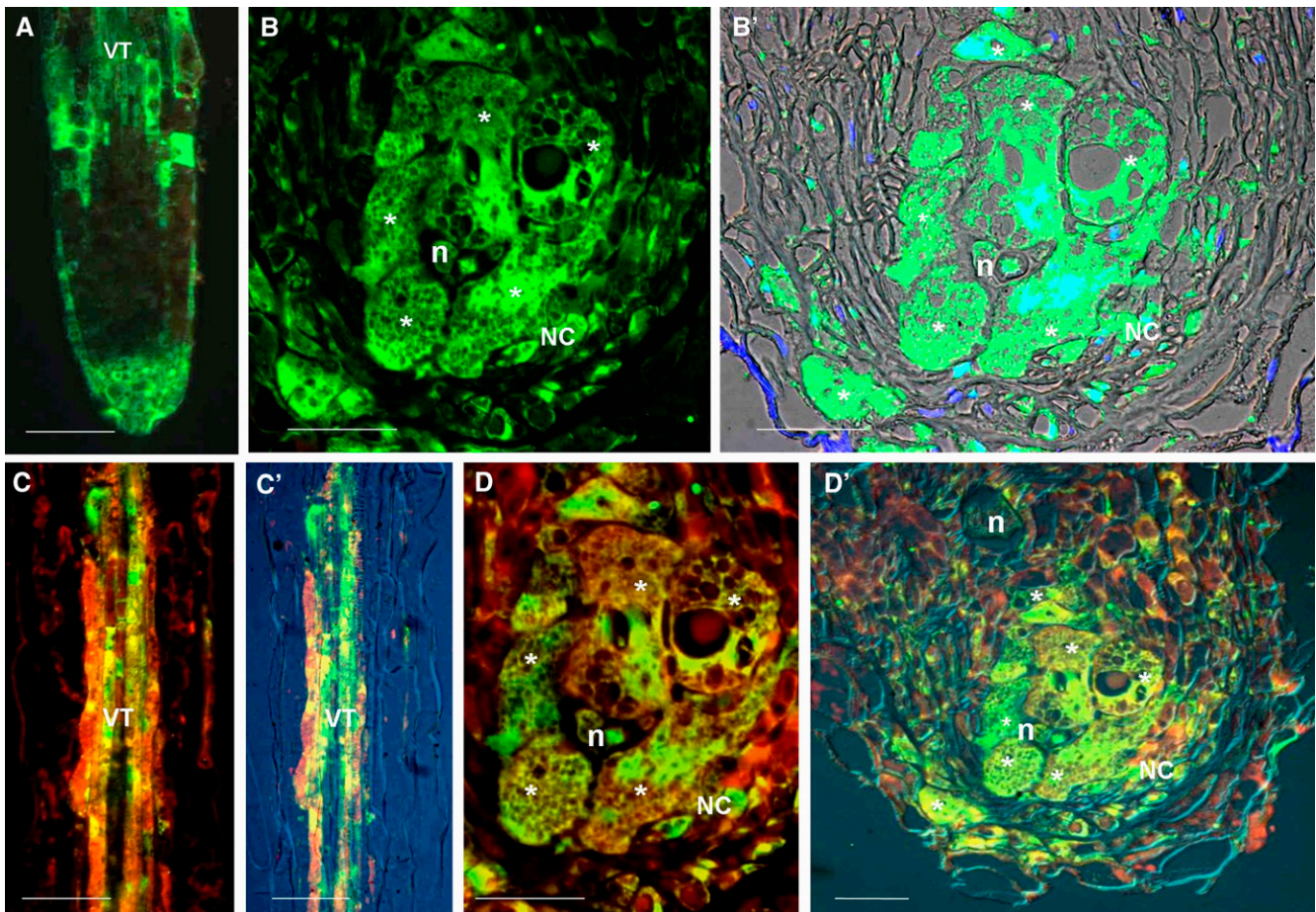


Figure 1. Nematode Infection Causes Increased ADF Immunostaining.

Immunostaining of uninfected roots [A], [C], and [C'] and galls 10 DAI [B], [B'], [D], and [D'] with anti-ZmADF3 (green; [A], [B], and [B']) or double localization of anti-ZmADF3 (green) and anti-actin (red; [C], [C'], [D], and [D']). (B'), (C'), and (D') are overlays of differential interference contrast transmission, 4',6'-diamidino-2-phenylindole-stained (blue; stains DNA), and immunolabeled images. Yellow coloring corresponds to the sites of ADF and actin colocalization. VT, vascular tissue; NC, neighboring cell; n, nematode, *, giant cell. Bars = 50 μ m.

and Northcote, 1972) that serve as the sole nutritive source for the nematode. Surrounding giant cells, neighboring cells divide asymmetrically, forming a typical root-knot or a gall. Although giant cells fully differentiate at early stages of nematode development, they only reach maximal size at the end of the nematode life cycle (Bird, 1971). Mature females then release hundreds of eggs into a proteinaceous matrix on the surface of the root that hatch into motile, second-stage (J2) juveniles, which usually reinfest the same plant.

A number of plant genes have been implicated in the reorganization of the giant cell actin cytoskeleton (Favery et al., 2004; Jammes et al., 2005). For example, three formin genes, *FH1*, *FH6*, and *FH10*, are induced in giant cells. *FH6* is distributed throughout the plasma membrane and may regulate giant cell isotropic growth by regulating the assembly of actin cables. These actin cables within giant cells may be required to guide vesicle trafficking that is needed for extensive plasma membrane and cell wall biogenesis during their isotropic growth (Favery et al., 2004). Chemical treatments blocking cytoskeleton dynamics result in the cessation of normal giant cell and nematode development (de Almeida Engler et al., 2004). Thus, reorganization of the cytoskeleton is implicated as a key aspect of giant cell formation and the successful completion of the nematode life cycle.

Here, we investigate the role of *ADF2* in root-knot nematode infection. ADF is upregulated in the giant feeding cells that develop after nematode infection, and an ADF family gene expression signature is apparent. In particular, *ADF2* is expressed throughout gall development and upregulated between 14 and 21 d after infection. Knockdown of *ADF2* using RNA interference (RNAi) has demonstrated the importance of this gene in normal plant development. Moreover, in infected plants, reduced levels of *ADF2* cause the net stabilization of F-actin in the initiated giant feeding cells, blocking cell maturation and consequently nematode development and reproduction. We suggest that upregulation of *ADF2* in the plant is an essential component of successful nematode infection.

RESULTS

ADF Localizes to the Giant Cell Cytoplasm and Nucleus

The distribution of ADF in uninfected roots and in galls was determined by immunofluorescence microscopy using a polyclonal antiserum against maize *ADF3* (Jiang et al., 1997), which cross-reacts with several *Arabidopsis* ADF isoforms (see Supplemental Figure 1 online). In control and nematode-infected roots, ADF was detected mainly in the elongation zone and root tip (Figure 1A), localizing in both cytoplasm and nuclei. A much stronger signal was observed in giant-feeding cells of *Arabidopsis* (Figures 1B and 1B'), tobacco (*Nicotiana tabacum*), and pea (*Pisum sativum*) infected by *M. incognita*. Double immunocytochemical staining of ADF and actin revealed that both proteins are present in the vascular tissues of uninfected roots (Figures 1C and 1C') and abundant in giant cells (Figures 1D and 1D'). Notably, actin staining by anti-actin was uniform in all gall cells (Figure 1D') and stronger than the ADF signal in the cells surrounding the feeding cells (Figures 1D and 1D'). In giant cells,

a higher concentration of ADF than actin was particularly seen in nuclei. This suggests that *ADF* expression is upregulated during feeding cell development.

Expression of ADF Genes in Galls

Noting that there were changes in the levels of ADF expression as observed by immunofluorescence, we investigated whether this correlated with changes in the transcription of *ADF* genes in response to *M. incognita* infection. We quantified the expression of seven *ADF* isoforms using quantitative RT-PCR in roots and galls 7, 14 and 21 d after inoculation (DAI; Figure 2). The transcript levels of five isoforms (*ADF2*, *ADF3*, *ADF4*, *ADF5*, and *ADF6*) were higher in galls of the infected roots compared with those of the control, and *ADF2* in particular exhibited a specific induction between 14 and 21 DAI. We examined GUS reporter translational fusion lines of *Arabidopsis ADF2*, *ADF3*, *ADF4*, *ADF6*, and *ADF10* (Ruzicka et al., 2007) and investigated the expression of these five *ADF_{pro}:GUS* lines in infected *Arabidopsis* plants. Our results show that *ADF2_{pro}:GUS* is expressed in the root vascular tissue (Figure 3A) and is highly induced in giant cells and neighboring cells at different time points after nematode inoculation (7, 14, and 21 DAI; Figures 3B to 3D). Increase of *ADF2* expression was not detected at 7 DAI during quantitative PCR analysis due to the high GUS staining in the vascular tissue of the uninfected root. *ADF2_{pro}:GUS* expression was induced at exceptionally high levels until the late stages of giant cell development. Interestingly, *ADF3_{pro}:GUS* and *ADF6_{pro}:GUS* were expressed in the vascular tissue of control roots (Figures 3E and 3M) and in some distal gall cells, but downregulated in giant cells (Figures 3F to 3H, 3O, and 3P). Although present throughout the root (Figure 3I), *ADF4_{pro}:GUS* expression decreased during nematode migration within the root (Figure 3J), and nearly no GUS

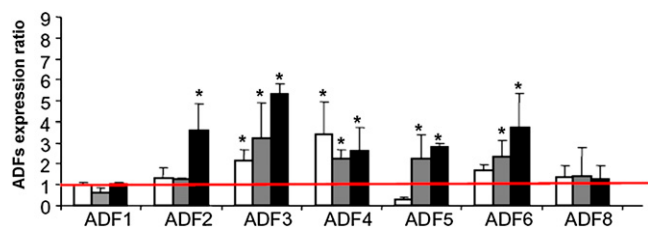


Figure 2. Analysis of Expression Levels of *ADFs* in Galls.

Relative amount of transcripts of *ADF1*, *ADF2*, *ADF3*, *ADF4*, *ADF5*, *ADF6*, and *ADF8* genes in *Arabidopsis* galls 7 (white bars), 14 (gray bars), and 21 (black bars) DAI with the nematode by quantitative RT-PCR in comparison to uninfected condition. The ratio was calculated as $2^{-(\Delta\Delta Ct)}$ gene of interest (Ct uninfected - Ct infected)/ $\Delta\Delta$ Ct reference gene (Ct uninfected - Ct infected), where the gene of interest is one of the analyzed *Arabidopsis ADF* genes (*ADF1-6* or *ADF8*) and the reference gene is *UBP22*. The ratio equals 1, meaning that the ADF gene is not regulated by nematode infection. Two biological replicates were performed. Three independent quantitative RT-PCR reactions were performed per sample. The bars (SE) represent mean values of two independent experiments. Statistical significance of the differences between dissected galls and control (nonmeristematic root fragments from noninfected plants) were determined by the Wilcoxon test (* $P < 0.05$).

[See online article for color version of this figure.]

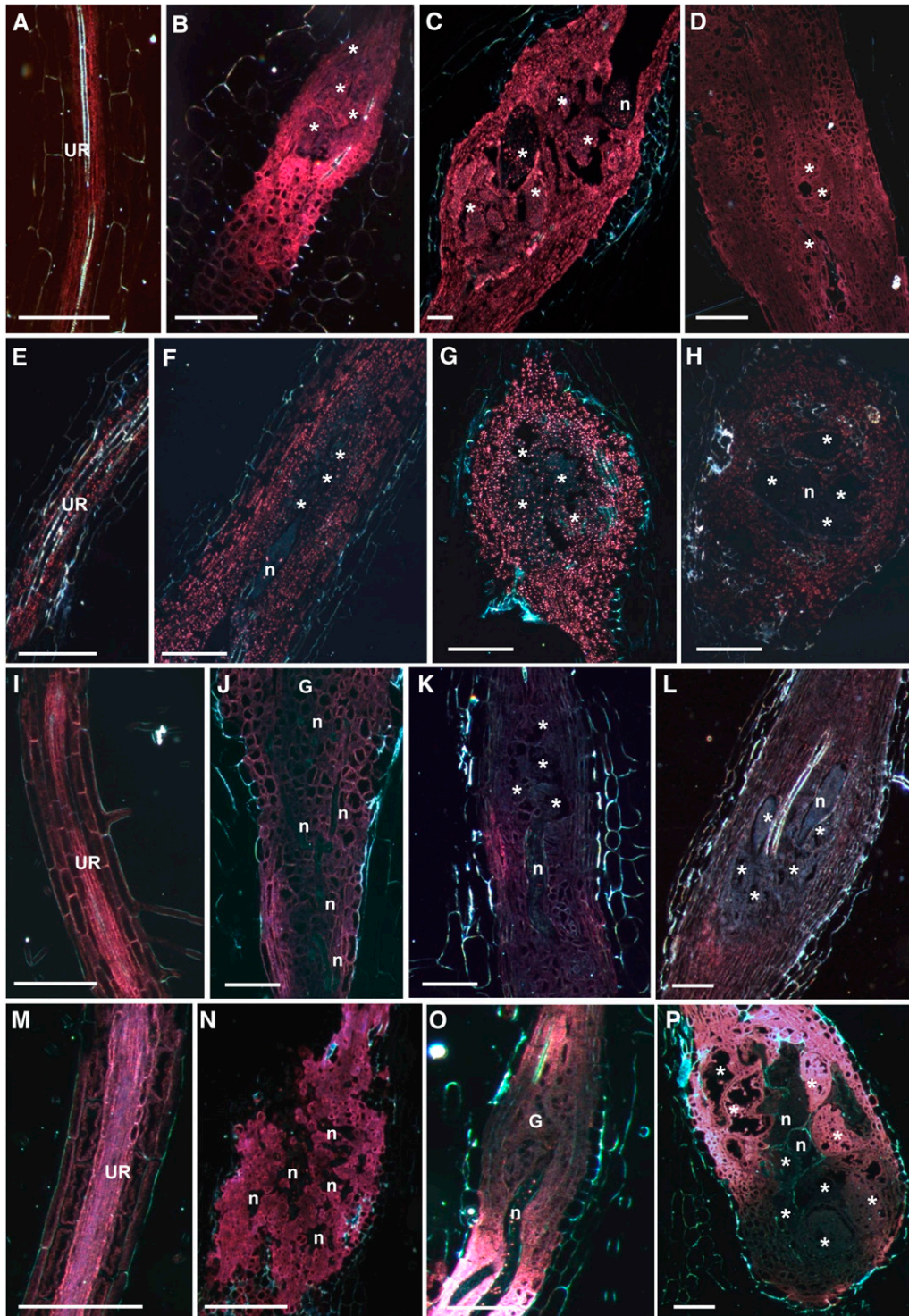


Figure 3. Expression Patterns of Four ADF_{pro} :GUS Lines in Galls Induced by *M. incognita* in *Arabidopsis* Roots.

Dark-field images illustrate GUS staining in red. UR, uninfected root; *, giant cell; n, nematode; G, gall. Bars = 100 μ m.

(A) $ADF2_{pro}$:GUS expression in uninfected roots.

(B) $ADF2_{pro}$:GUS expression in galls induced by *M. incognita* 7 DAI.

(C) $ADF2_{pro}$:GUS expression in galls induced by *M. incognita* 14 DAI.

(D) $ADF2_{pro}$:GUS expression in galls induced by *M. incognita* 21 DAI.

expression was observed in giant cells in contrast to neighboring cells (Figures 3K and 3L). *ADF6_{pro}*:GUS expression was strong in the vascular tissue of uninfected roots (Figure 3M) and stayed active during nematode migration (Figure 3N). *ADF6_{pro}*:GUS expression in giant cells was weak at 7 DAI (Figure 3O) and further diminished toward 14 (Figure 3P) and 21 DAI.

Downregulation of ADF2 Affects Plant Development

As the *ADF2* transcript level is upregulated in *Arabidopsis* during nematode infection and its expression is concentrated in the giant cells, we investigated the effect of knocking down the *ADF2* transcript levels (7, 14, and 21 DAI) during nematode infection using ethanol-inducible *ADF2*-RNAi lines. The amount of *ADF2* transcript, but not the transcript from the other *ADF* genes, was reduced in the ethanol-induced *ADF2*-RNAi seedlings (Figure 4). Induction of the *ADF2*-RNAi caused a range of cellular defects compared with controls. The leaves had yellowing regions and they were more serrated at the circumference (Figure 5A). The leaf morphology of uninduced (Figure 5B) and ethanol-treated wild-type *Arabidopsis* (Columbia-0 [Col-0]) was normal. The yellowing regions on the leaves of the induced *ADF2*-RNAi seedlings correlated with necrotic palisade parenchyma cells and an enlargement of cells surrounding the vascular bundles (cf. Figures 5E and 5F). Siliques from induced *ADF2*-RNAi seedlings are small, shrunken, and bent, often failing to penetrate through the layers of petals and sepals, and produce fewer fertile seeds (9 to 16 seeds per silique) compared with control seedlings (42 to 54 seeds per silique; Figures 5C and 5D). The morphology of other aerial organs was not visibly affected after *ADF2*-RNAi induction. The reduced growth of siliques in *ADF2* knockdown lines is indicative of defective embryogenesis. In siliques from control plants (Figures 5G and 5I to 5K), all stages of embryo development starting from globular to late heart stage were present (Figures 5I to 5K). In siliques of plants with *ADF2* levels reduced (1 to 2 weeks after flowering), we observed seeds in different developmental stages. Some embryo sacs appeared unfertilized (Figure 5H), while others were aborted at the zygote or a two-cell pro-embryo stage (Figures 5L to 5N). As a result, very few seeds developed normally in induced *ADF2*-RNAi plants.

A detailed morphological analysis was performed on in vitro-grown seedlings (Figure 6). The shoot apical meristem did not show clear anatomical defects. It contained the typical three layers

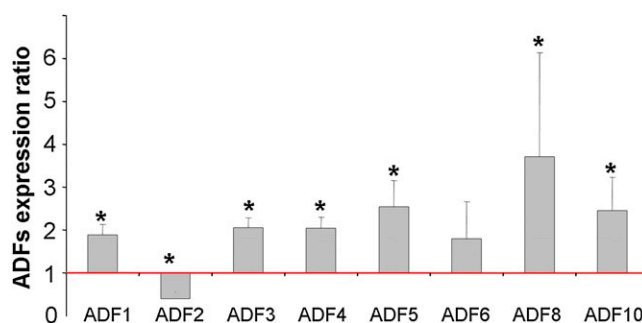


Figure 4. Analysis of Expression Levels of *ADFs* in the Ethanol-Inducible *ADF2*-RNAi Line.

Quantitative RT-PCR expression analysis of eight *Arabidopsis ADF* genes (*ADF1*, *ADF2*, *ADF3*, *ADF4*, *ADF5*, *ADF6*, *ADF8*, and *ADF10*) in the ethanol-induced *ADF2* knockdown line showing the specific downregulation of the *ADF2* gene in whole seedlings 15 d after sowing in comparison with noninduced. The ratio was calculated as $2^{-(\Delta\Delta Ct \text{ gene of interest})}$ (Ct ethanol noninduced - Ct ethanol induced)/ $\Delta\Delta Ct \text{ reference gene}$ (Ct ethanol noninduced - Ct ethanol induced), where the gene of interest is one of the *Arabidopsis ADF* genes (*ADF1-6*, *ADF8*, or *ADF10*) and the reference gene is *UBP22*. The ratio is ≥ 1 , meaning that the gene is not downregulated by the ethanol treatment. Two biological replicates were performed. Three independent quantitative RT-PCR reactions were performed per sample. The bars (SE) represent mean values from two independent experiments. Statistical significance of the differences between 15-d-old noninduced and ethanol-treated *ADF2*-RNAi line seedlings was determined by Wilcoxon test (* $P < 0.05$). [See online article for color version of this figure.]

as seen for the wild-type meristem in a flattened to domed shape. The pith tissue located just below the rib meristem is less organized in the induced *ADF2*-RNAi line, and the central cylinder just below is wider (see Supplemental Figure 2 online). Leaf sections of in vitro-grown seedlings showed that the venation system was often thicker with wider cells (five cell layers; Figure 6A) compared with control sections (three to four cell layers; Figure 6B, Table 1). In addition, the surrounding cell files were composed of cells with a dense cytoplasm and enlarged nuclei of diameter of 10 to 16 μm (Figure 6A) compared with 6 to 7 μm for the same cells in controls (Figure 6B). Mesophyll tissue showed wider intercellular spaces compared with controls and seemed to contain more plastids. The root central cylinder was wider, containing more cell files (eight to

Figure 3. (continued).

- (E) *ADF3_{pro}*:GUS expression in uninfected roots.
- (F) *ADF3_{pro}*:GUS expression in galls induced by *M. incognita* 7 DAI.
- (G) *ADF3_{pro}*:GUS expression in galls induced by *M. incognita* 14 DAI.
- (H) *ADF3_{pro}*:GUS expression in galls induced by *M. incognita* 21 DAI.
- (I) *ADF4_{pro}*:GUS expression in uninfected roots.
- (J) *ADF4_{pro}*:GUS expression in galls induced by *M. incognita* 7 DAI.
- (K) *ADF4_{pro}*:GUS expression in galls induced by *M. incognita* 14 DAI.
- (L) *ADF4_{pro}*:GUS expression in galls induced by *M. incognita* 21 DAI.
- (M) *ADF6_{pro}*:GUS expression in uninfected roots.
- (N) *ADF6_{pro}*:GUS expression in during nematode migration.
- (O) *ADF6_{pro}*:GUS expression in galls induced by *M. incognita* 7 DAI.
- (P) *ADF6_{pro}*:GUS expression in galls induced by *M. incognita* 14 DAI.

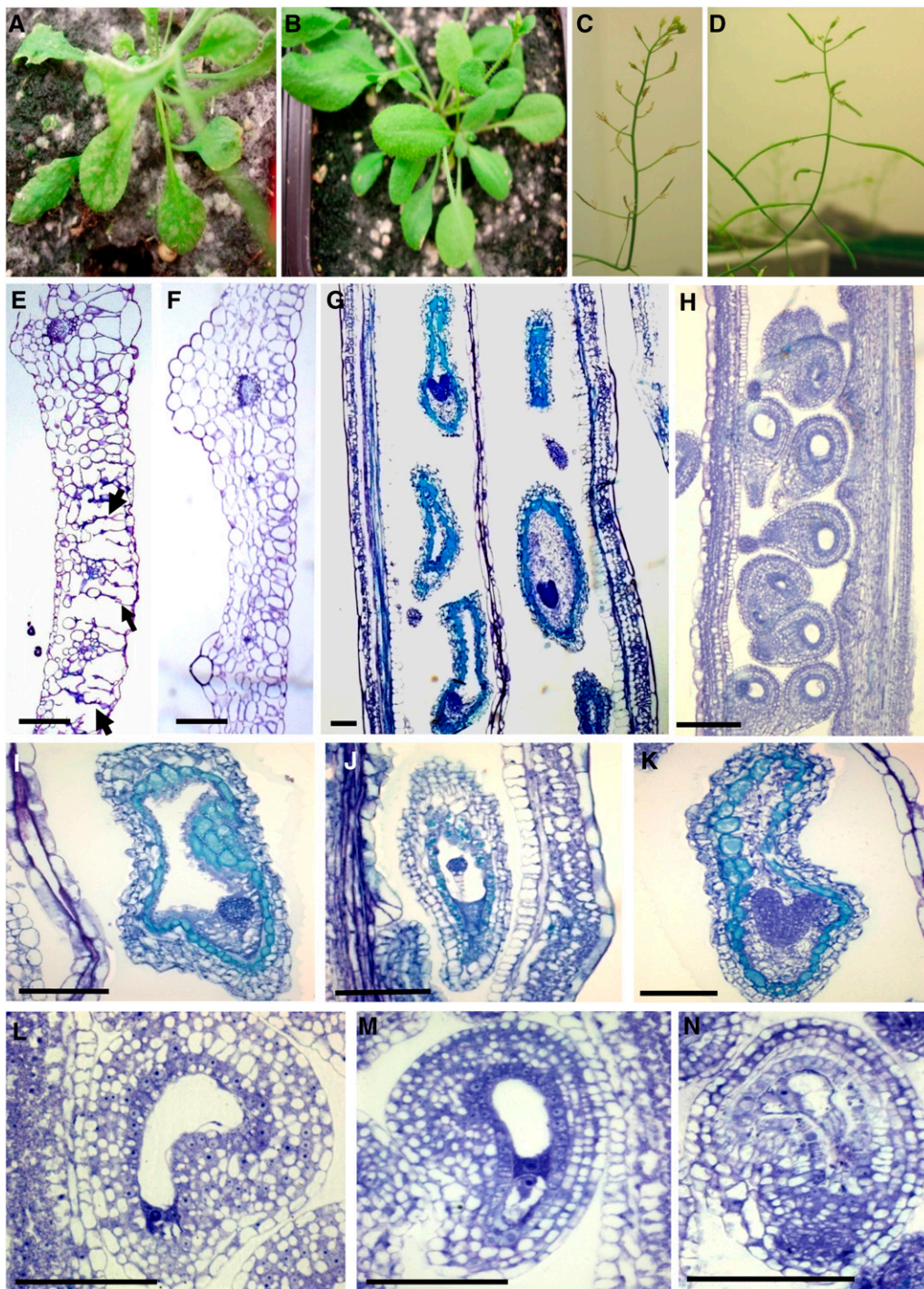


Figure 5. Morphological Analysis of the *ADF2* Knockdown Line and Noninduced Control Seedlings.

Bright-field micrographs of tissue sections stained with toluidine blue ([E] to [N]). Bars = 100 μ m.

(A) Ethanol-induced *ADF2*-RNAi plants showing yellow spots in the leaves.

(B) Noninduced *ADF2*-RNAi plants.

(C) Ethanol-induced *ADF2*-RNAi plants showing disruptions in silique growth.

(D) Siliques of noninduced *ADF2*-RNAi plants.

(E) Section through a leaf of an ethanol-induced *ADF2*-RNAi plant showing necrotic regions (arrows) in the mesophyll.

(F) Section through a leaf of a noninduced *ADF2*-RNAi plant.

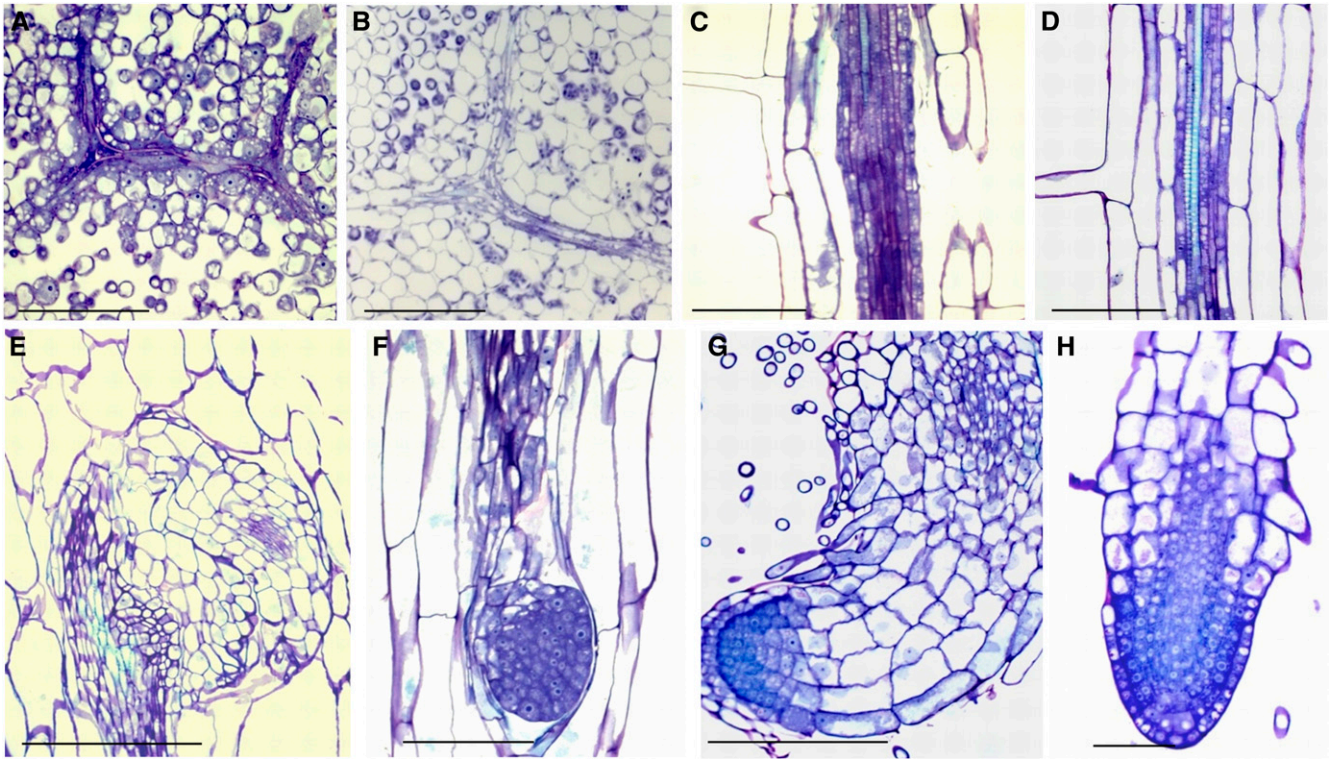


Figure 6. Morphological Analysis of the *ADF2* Knockdown Line and Noninduced Control Seedlings.

Bright-field micrographs of longitudinal tissue sections stained with toluidine blue. Bars = 50 μm .

(A) Section through a leaf of an ethanol-induced *ADF2*-RNAi seedling 16 d after sowing (DAS), showing a thickening of the vascular tissue.

(B) Section through a leaf of a control noninduced *ADF2*-RNAi seedling 16 DAS.

(C) Section through a root of an ethanol-induced *ADF2*-RNAi seedling 16 DAS, showing a thickening of the vascular tissue.

(D) Section through a root of a control noninduced *ADF2*-RNAi seedling 16 DAS.

(E) Section through a root lateral meristem in an ethanol-induced *ADF2*-RNAi seedling 16 DAS.

(F) Section through a root lateral meristem of a control noninduced *ADF2*-RNAi seedling 16 DAS.

(G) Section through a root meristem of an ethanol-induced *ADF2*-RNAi seedling 16 DAS.

(H) Section through a root meristem of a control noninduced *ADF2*-RNAi seedling 16 DAS.

nine cell layers) and wider cells with a dense cytoplasm (Table 1, Figure 6C) compared with the control (five to six cell layers; Figure 6D). A set of lateral root meristems from ethanol-induced *ADF2*-RNAi seedlings showed the ectopic appearance of lateral roots (Figure 6E) compared with noninduced roots (Figure 6F). Lateral roots emerged malpositioned associated to the vascular tissue in comparison with normally developed roots. In addition, ethanol-induced plants occasionally had smaller root apical meristems (Figure 6G) compared with control roots (Figure 6H). Ethanol-treated wild-type *Arabidopsis* seedlings (Col-0) displayed a normal leaf and root anatomy, as observed for untreated control *ADF2*-RNAi seedlings.

Actin Organization Is Altered in Ethanol-Induced *ADF2*-RNAi Seedlings

We investigated the effect of *ADF2* knockdown on F-actin organization in 7- and 16-d-old seedlings (Figures 7A to 7D) expressing the actin marker, fimbrin actin binding domain 2 fused to green fluorescent protein (*GFP:FABD2*; Ketelaar et al., 2004). Young ethanol-induced *ADF2*-RNAi seedlings (7 d after germination) showed an overall brighter actin network (Figure 7A) compared with noninduced seedlings (Figure 7E), suggesting that the actin cytoskeleton is stabilized upon *ADF2* suppression. Generally, a reduction in *ADF2* resulted in a denser F-actin

Figure 5. (continued).

(G) Section through a silique of a noninduced *ADF2*-RNAi plant.

(H) Section through a silique of an ethanol-induced *ADF2*-RNAi plant showing unfertilized ovules.

(I) to (K) Sections through fertilized ovules in a control noninduced *ADF2*-RNAi silique at globular [(I) and (J)] and heart stages (K).

(L) to (N) Sections through fertilized ovules of an ethanol-induced *ADF2*-RNAi silique showing a zygote, a two-cell stage pro-embryo, and a malformed embryo.

Table 1. Average Length in μm ($\pm\text{SD}$) of Leaf Vascular Bundles and Cell Size and Root Vascular Tissue Diameter and Cell Size of 16-d-Old Ethanol-Induced and Noninduced *ADF2*-RNAi Seedlings

		<i>ADF2</i> -RNAi Induced Line	<i>ADF2</i> -RNAi Noninduced Line
Leaf	Vascular bundles	29.9 \pm 4.8	16.8 \pm 1.6 ^a
	Cell width	7.6 \pm 0.7	4.1 \pm 0.7 ^a
Root	Total root	155.5 \pm 17.5	126.7 \pm 14.6 ^a
	Vascular cylinder	57.0 \pm 7.0	38.4 \pm 6.5 ^a
	Cell width	9.6 \pm 2.5	4.9 \pm 1.1 ^a

^aStatistically significant differences for values compared with the *ADF2*-RNAi noninduced line were determined by Student's *t* test ($P < 0.01$).

network in cotyledons (Figure 7B) and caused the accumulation of actin filaments around the nucleus in hypocotyl epidermal cells (Figure 7C). A greater number of actin bundles were also observed throughout most of the root vascular tissue (Figure 7D). Cells in similar control tissues showed a less dense actin cytoskeleton (Figures 7E to 7H). Actin bundle thickness was similar in control and ethanol-treated samples (minimal width of 0.4 μm), indicating that lack of *ADF2* does not affect the thickness of actin bundles. To further investigate how *ADF2* affects the actin cytoskeleton, we compared the organization of the actin cytoskeleton in *ADF2*-deficient plants (Figures 7I and 7K) with control seedlings (Figures 7J and 7L) when both were treated with 5 μM latrunculin B (LatB). LatB prevents the polymerization of new actin filaments from a dynamic pool of monomeric actin generated from the turnover of F-actin (Ayscough et al., 1997). One hour after the application of LatB, a few disorganized actin filaments were detected in the control plants, whereas we observed little decrease in the amount of F-actin in the *ADF2*-deficient plants. These data suggest that the actin network is not being dynamically remodeled in the absence of *ADF2*.

Downregulation of *ADF2* Inhibits Nematode Feeding Site Development

To investigate the effect of *ADF2* knockdown on the process of nematode infection, we performed a morphological analysis of galls at different developmental stages. Nematode infection tests were conducted to evaluate the efficiency of nematode development and reproduction in ethanol-induced and non-induced *ADF2*-RNAi seedlings and Col-0 ethanol-treated and untreated seedlings. Knockdown of *ADF2* had no visible effect on the ability of nematodes to penetrate, migrate, and induce giant cells; however, morphological analysis showed that in comparison to noninduced roots, there is a delay in feeding site development already observed at 7 DAI. While the cytoplasm of control giant cells is dense, containing numerous large nuclei (Figure 8A), giant cells in plants with low levels of *ADF2* often contain only one nucleus, are filled with small vacuoles, and have less dense cytoplasm (Figures 8B and 8B'). In ethanol-induced *ADF2*-RNAi roots at 14 DAI, the nematodes remained at stage 2 juvenile (J2) while the giant cells only developed to the binucleate stage. This characteristic stage is normally only observed during the first hour after infection. At 21 DAI, wild-type giant cells

showed the typical multinucleated cells with dense cytoplasm (Figure 8C), and mature nematodes had developed. At this same stage in infected roots of seedlings where *ADF2* expression was reduced, the feeding cells were small and had few nuclei (Figures 8D and 8D') and the nematodes were arrested in their development at the juvenile stage. The number of nuclei in giant cells of the ethanol-induced seedlings of the *ADF2*-RNAi line was always significantly lower (approximately two nuclei per giant cell) in comparison to noninduced samples containing around 50 nuclei. The number of nuclei was determined throughout the whole depth of the feeding sites using serial sections stained with toluidine blue or 4',6-diamidino-2-phenylindole and by differential interference contrast imaging of thick fresh vibroslices.

Nematode infection tests showed that the development of the majority of the galls was arrested in the ethanol-induced *ADF2*-RNAi line. Moreover, the vast majority of nematodes did not mature and were unable to produce egg masses (Figures 9A and 9B). It should be noted that a small number of nematodes do develop and survive, and this is due to the low concentration of ethanol used to keep the *ADF2*-RNAi plants just healthy enough for these long-term infection experiments (2 months). Similar control experiments using noninduced *ADF2*-RNAi seedlings (Figures 9A and 9B) showed normal nematode maturation and egg mass production. Treatment of control Col-0 seedlings with ethanol had no effect on gall development, indicating that this effect is indeed the result of the downregulation of *ADF2* and not the presence of ethanol.

Actin Organization Is Altered in Giant Cells When *ADF2* Levels Decline

In vivo examination of the actin cytoskeleton using the actin decorating GFP-FABD fusion protein in ethanol-induced *ADF2*-RNAi seedlings has shown the unusual appearance of actin bundles throughout the root cells. The root vascular cylinder cells have a denser network of actin bundles (Figure 10A) compared with noninduced plants (Figure 10D). Selected parenchyma cells of the vascular tissue are the focal targets of root-knot nematodes. Nematode infection of ethanol-induced *ADF2*-RNAi lines resulted in an increased number of actin bundles and thicker cables throughout the cortex and cytoplasm of often binucleate giant cells 10 to 21 DAI (Figures 10B, 10C, and 10C'). By contrast, noninduced *ADF2*-RNAi feeding cells always harbored multiple nuclei and relatively sparse cables throughout the cytoplasm with dominant dense bundles and filaments distributed throughout the giant cells 10 DAI (Figures 10E and 10E'). The difference in gall size is notable between induced and noninduced *ADF2*-RNAi infected roots. Induced galls with reduced *ADF2* levels were significantly smaller and contained less but larger neighboring cells (Figure 10C) than those in control plants (Figure 10E).

DISCUSSION

ADF Expression during Nematode Infection

Immunolocalization of *ADF* in nematode-infected *Arabidopsis* roots indicated that *ADF* is upregulated in the giant feeding cells

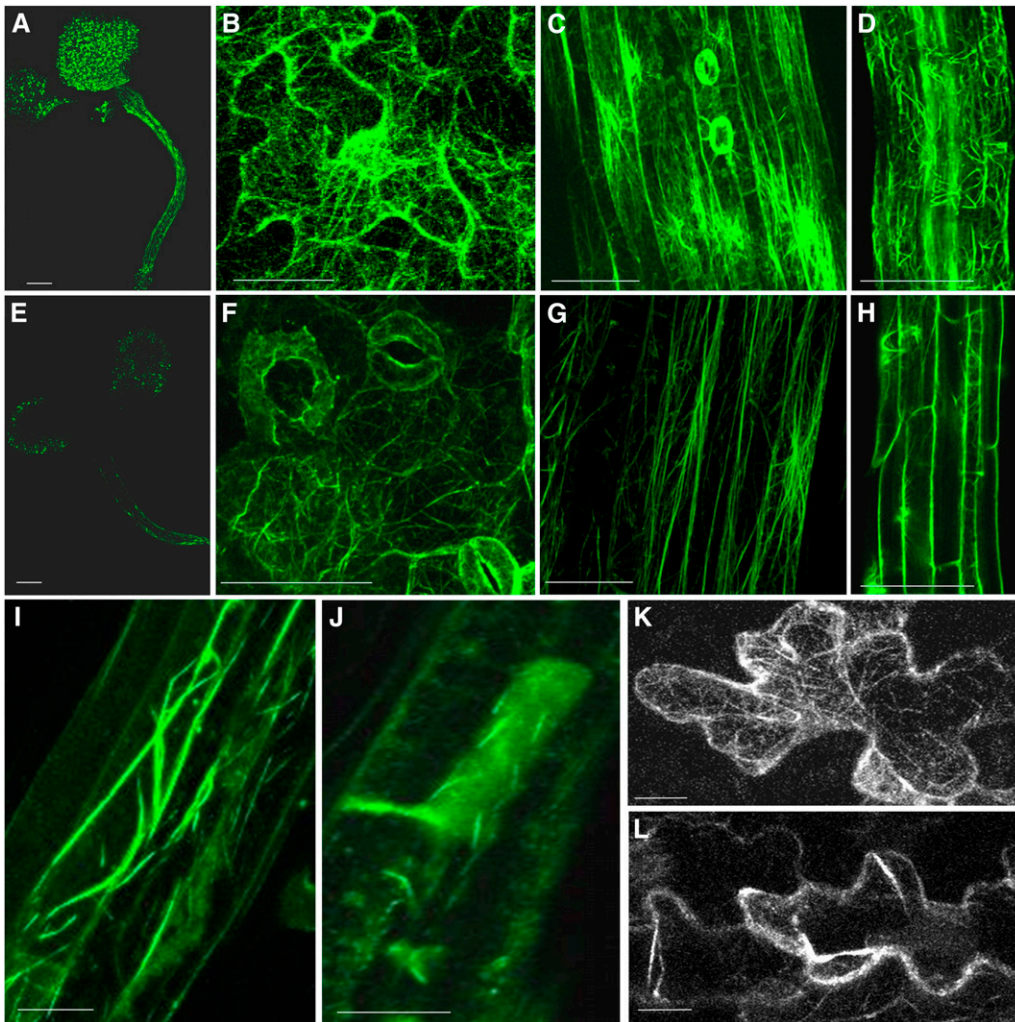


Figure 7. Effect of *ADF2* Knockdown on Actin Organization.

Actin cytoskeleton (green) reorganization in *ADF2*-RNAi seedlings with and without LatB treatment. The actin cytoskeleton in ethanol-induced *ADF2*-RNAi cells displays condensed bundles and thick cables of F-actin. Projections of serial confocal optical sections are shown. Bars = 200 μ m in (A) and (E), 20 μ m in (B) and (I) to (L), and 100 μ m in (C), (D), and (F) to (H).

(A) Ethanol-induced *ADF2*-RNAi seedling 7 DAS, showing a dense actin cytoskeleton.

(B) Leaf epidermis of an ethanol-induced *ADF2*-RNAi seedling 16 DAS, showing dense actin filaments.

(C) Hypocotyl of an ethanol-induced *ADF2*-RNAi seedling 16 DAS, showing dense actin filaments.

(D) Root of an ethanol-induced *ADF2*-RNAi line, showing densely packed actin bundles within the vascular tissue.

(E) Control noninduced *ADF2*-RNAi seedling 7 DAS.

(F) Leaf epidermis of control noninduced *ADF2*-RNAi line 16 DAS.

(G) Hypocotyl of a control noninduced *ADF2*-RNAi seedling 16 DAS.

(H) Root of a control noninduced *ADF2*-RNAi seedling, showing filamentous actin mainly surrounding the nucleus.

(I) LatB-treated root cell of an ethanol-induced *ADF2*-RNAi seedling, showing resistance to actin depolymerization.

(J) LatB-treated root cell of a control noninduced *ADF2*-RNAi seedling, showing the depolymerized actin cytoskeleton.

(K) LatB-treated leaf cell of an ethanol-induced *ADF2*-RNAi seedling, showing resistance to actin depolymerization.

(L) LatB-treated leaf cell of a control noninduced *ADF2*-RNAi seedling, showing the depolymerized actin cytoskeleton.

that originate from nematode-targeted root parenchymal cells of the vascular cylinder. Further analysis of the transcription profiles of several *ADF* genes revealed that in the course of infection over 21 d, a specific *ADF* family expression signature was observed. Quantitative RT-PCR results showed that most *ADFs* are ex-

pressed in nematode-induced galls; however, the transcription of five genes (*ADF2*, 3, 4, 5, and 6) was significantly increased. Out of these five, only *ADF2* was expressed at early stages of infection and induced at the later stages of infection (14 to 21 DAI). GUS analysis of nematode-infected roots was performed to

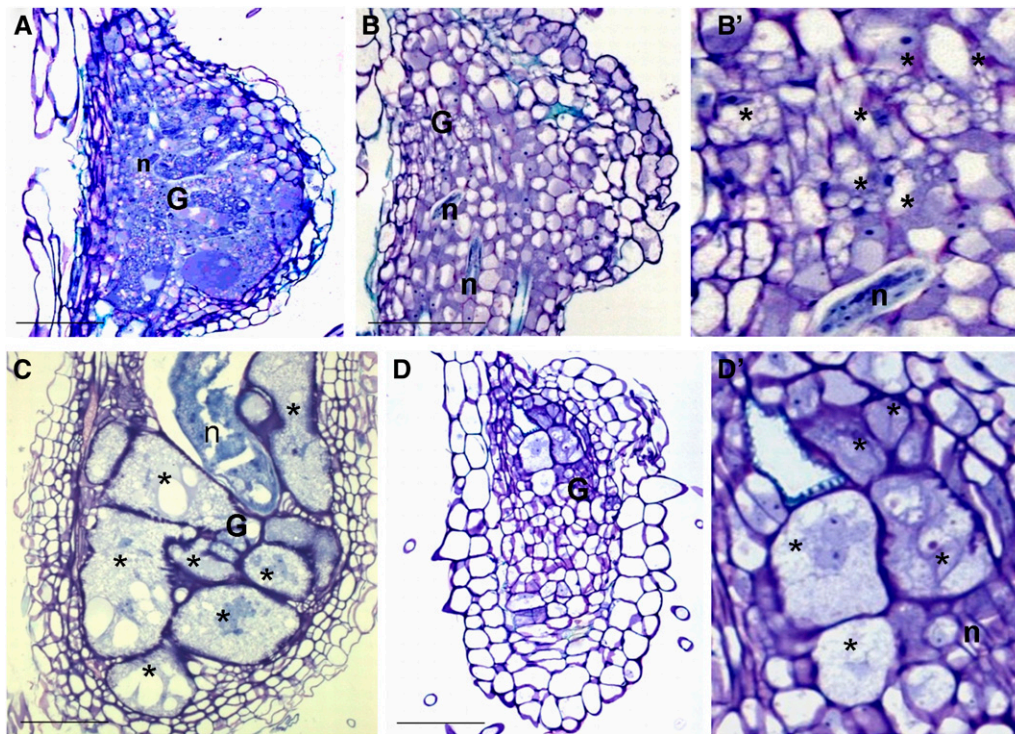


Figure 8. Morphological Analysis of Galls in *ADF2* Knockdown Line and Noninduced Nematode-Infected Control Roots.

Bright-field micrographs of sections stained with toluidine blue. Histological analysis of ethanol-induced *ADF2*-RNAi galls (**[B]**, **[B']**, **[D]**, and **[D']**) compared with noninduced *ADF2*-RNAi control galls (**[A]** and **[C]**). Tissue sections through galls 7 DAI from a control noninduced (**[A]**) and ethanol-induced *ADF2*-RNAi (**[B]** and **[B']**) show that giant cell development is blocked when *ADF2* is downregulated. Sections through galls 21 DAI from a noninduced control (**[C]**) and ethanol-induced *ADF2*-RNAi (**[D]** and **[D']**). Detail of a gall (**[D']**) shows giant cells arrested at the binucleate stage. G, gall; n, nematode; *, giant cell. Bars = 50 μ m.

determine in which gall cells *ADFs* are expressed. These assays demonstrated that only the *ADF2_{pro}:GUS* construct was highly active in giant cells induced by root-knot nematode *M. incognita*, while the activity of *ADF3_{pro}:GUS*, *ADF4_{pro}:GUS*, and *ADF6_{pro}:GUS* was concentrated in the neighboring cells. Interestingly, *ADF4_{pro}:GUS* is significantly downregulated in giant cells but not in the flanking vascular root cells at all stages of gall development. By contrast, *ADF2_{pro}:GUS* is expressed in giant and neighboring cells at different stages of gall development (7 to 21 DAI). Specific upregulation of *ADF2* in giant cells during the later stages of infection suggests that this isotype has an important role during gall formation and development. *ADF3* expression has been observed in microarray studies of isolated feeding sites, and *ADF3* promoter activity has been reported in the root vascular tissue and in whole feeding sites induced by root-knot and cyst nematodes (Fuller et al., 2007). Our results of sectioned galls show that *ADF3*, *ADF4*, and *ADF6* are either weakly expressed or not expressed at all in giant cells, and stronger *ADF_{pro}:GUS* expression of these genes was observed in neighboring cells, suggesting that the function of these isotypes will not be redundant with respect to *ADF2*.

ADF was detected in the cytoplasm and nuclei of the giant cells by immunofluorescence microscopy. *ADF* located to regions where dynamic actin is expected, as previously observed for the site of root hair initiation and root hair tip growth (Jiang et al.,

1997). Moreover, *ADF/cofilin* has been implicated in nuclear function as it can be translocated into the nucleus in response to a variety of stresses, and this accumulation is correlated with a similar nuclear accumulation of actin (Nishida et al., 1987; Jiang et al., 1997; Pendleton et al., 2003). For example, *ADF* might shuttle actin into the nucleus or regulate gene expression at the chromatin level and the epigenetic determination of cell fate (Bettinger et al., 2004; Burgos-Rivera et al., 2008). Data on nuclear activities for actin and ABPs like *ADF* suggest the existence of a crucial crosstalk between nuclear and cytoplasmic compartments (Minakhina et al., 2005). Localization of *ADF* in the cytoplasm and nucleus of giant and neighboring cells might help to mediate a cellular stress response, regulate nuclear processes, and provide both compartments with relevant signals, such as the status of expanding cells (i.e., giant cells) and dividing cells (i.e., neighboring cells). Therefore, *ADF/cofilins* have the potential to alter gene expression and regulate plant development via their activities in either the nucleus or the cytoplasm.

***ADF2* Knockdown Causes Cellular Defects and Prevents Successful Nematode Infection**

As *ADF2* is expressed early during nematode infection and is upregulated between 14 and 21 DAI, we chose to investigate the

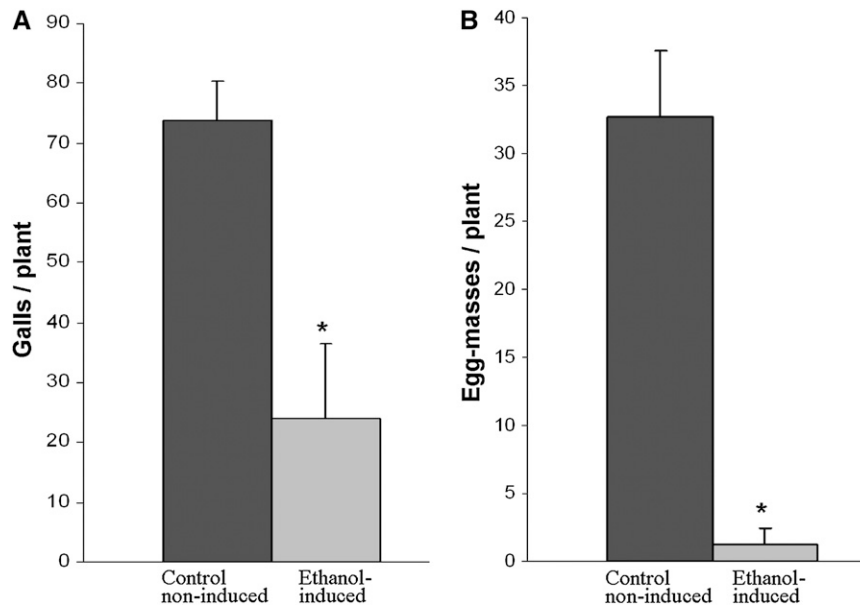


Figure 9. Nematode Infection Test in *ADF2* Knockdown Line.

Resistance test of ethanol-induced *ADF2*-RNAi seedlings (light-gray bars) to nematodes shows that the number and size of galls are significantly decreased (**A**) and nearly no egg masses are formed (**B**) compared with control noninduced *ADF2*-RNAi, infected *Arabidopsis* roots (dark-gray bars). Data shown represent means \pm SD from at least two experiments in which a minimum of 50 seedlings of each line were evaluated for nematode infection. * Statistically significant differences were determined by the Student's *t* test ($P < 0.01$).

function of this protein in feeding site development. We used an RNAi strategy to knock down the transcript levels of *ADF2*. We analyzed the phenotype of these plants and report cellular defects that are consistent with aberrations of the actin network. Furthermore, we report that knockdown of *ADF2* arrests giant cell development and consequently prevents the proliferation of root-knot nematodes.

ADFs function in the remodeling of the actin cytoskeleton by promoting severing and depolymerization of actin at the pointed end of the filaments in response to a wide variety of environmental and physiological signals (Bamburg, 1999). It is not surprising that knockout or knockdown of ADF in phylogenetically divergent organisms leads to abnormal actin organization and dynamics and can cause cell death (Augustine et al., 2008; Van Troys et al., 2008). Genetic studies of ADF in *Arabidopsis* have been complicated due to the relatively large gene family that consists of 11 genes (Dong et al., 2001a; Ruzicka et al., 2007) with different, but overlapping, expression programs. Detailed analysis of ADF transcription programs in *Arabidopsis* identified four subclasses (Ruzicka et al., 2007): subclass I (*ADF1*, 2, 3, and 4) is transcribed in all tissues and cell types, except pollen; members of subclass II are specific to pollen (*ADF7* and 10) and root trichoblast (*ADF8*); members of subclass III (*ADF5* and 9) have nonoverlapping transcription patterns in several organs and tissues, including the meristematic regions; and *ADF6* in subclass IV has a weak constitutive expression pattern in all tissues examined. Although there is limited data on the comparison of the biochemical activities of different ADF isoforms, the conservation of their primary sequences as well as their overlapping transcription activity suggest partial functional redundancy

within the gene family (Dong et al., 2001b; Ruzicka et al., 2007). Analysis of the individual gene knockouts and knockdowns is in agreement with this suggestion. For example, knockout of ubiquitously expressed *Arabidopsis ADF1* promotes the formation of a more interconnected network of actin cables in hypocotyl cells and root hairs but causes only a moderate phenotype (Dong et al., 2001b). In another case, lack of *Arabidopsis ADF9* resulted in abnormal F-actin growth, aberrant branching and filament structure in cells within the shoot apical meristem causing aberrant cytokinesis, and abnormal cell and organ expansion (Burgos-Rivera et al., 2008); however, these defects did not significantly affect normal plant development (Kandasamy et al., 2007).

Knockdown of *Arabidopsis ADF2* caused the accumulation of actin bundles in cells of the shoot apex, cotyledons, leaf tissues, and hypocotyls, especially in the vascular tissues, similar to knockout of *Arabidopsis ADF1*, suggesting that F-actin dynamics are compromised. To test this hypothesis, we treated leaves and roots of ethanol-induced *ADF2*-RNAi plants with LatB, a drug that sequesters actin monomers and thereby induces the depolymerization of dynamic actin filaments (Yormola et al., 2000). In contrast with control samples where most of the F-actin was depolymerized, actin bundles, to a large extent, were preserved in *ADF2*-depleted plants, indicating that knockdown of *ADF2* results in slower F-actin turnover. These data agree with the main activity of ADF/cofilins, namely to increase actin filament turnover (Carlier et al., 1997; Maciver, 1998; McGough et al., 2001) by severing actin filaments and increasing the rate at which actin monomers dissociate from the pointed end of the filaments (Mabuchi, 1983; Lappalainen and Drubin, 1997;

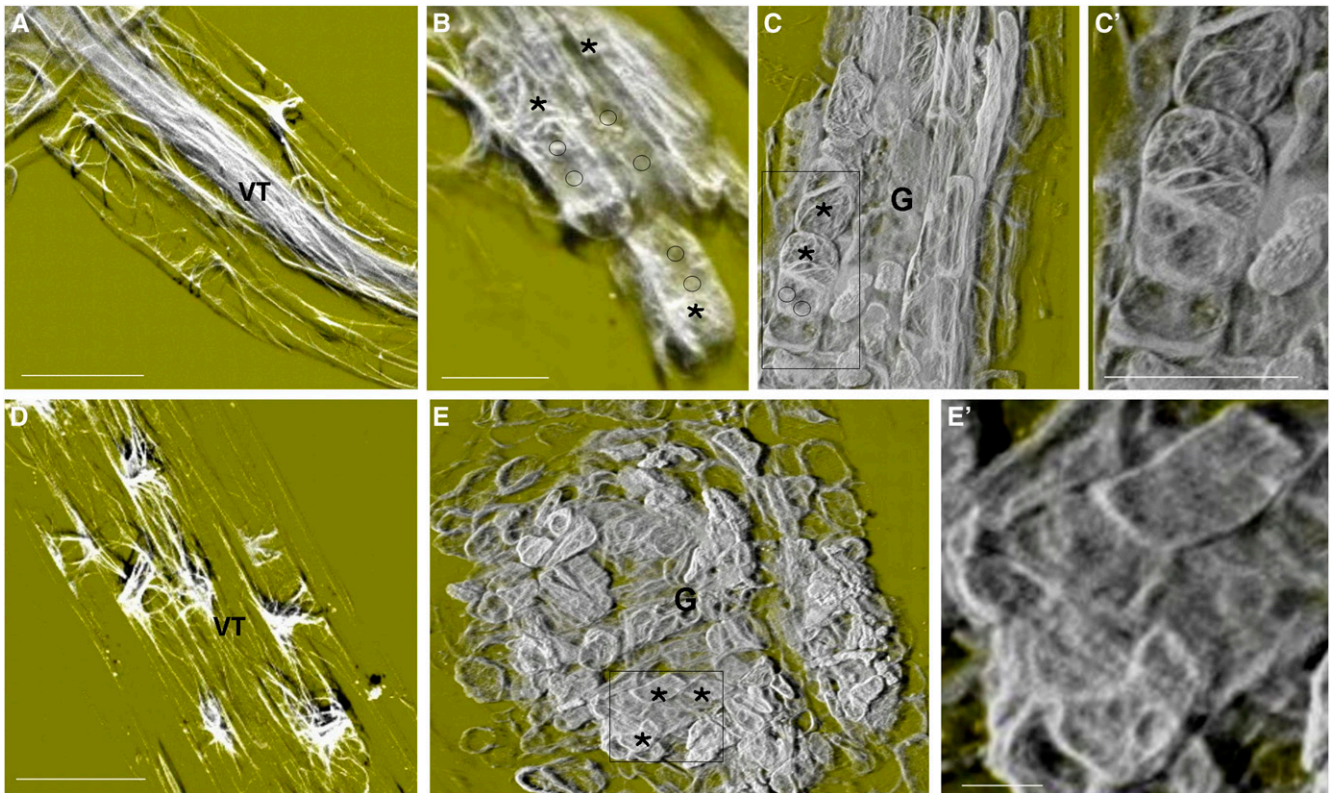


Figure 10. Actin Cytoskeleton Organization in Uninfected Roots and Galls of Ethanol-Induced *ADF2*-RNAi Seedlings and in Control Noninduced *ADF2*-RNAi Samples.

(A) to (C) Ethanol-induced uninfected root of *ADF2*-RNAi plant showing dense actin cables in the vascular tissue (A) and the dense actin network in giant cells and neighboring cells 10 (B) and 21 DAI (C).

(C') Detail of thick cables throughout the cytoplasm of giant cells arrested in their development corresponding to the boxed region in (C).

(D) Actin distribution in control noninduced *ADF2*-RNAi roots.

(E) and (E') Gall in control noninduced *ADF2*-RNAi root 10 DAI (E) and a detail (E') showing the thinner bundles throughout giant cells compared with induced giant cells corresponding to the boxed region in (E).

VT, vascular tissue; G, gall; *, giant cell; circles are nuclei of giant cells. Images were generated from serial confocal optical sections using shadow three-dimensional projection to better appreciate actin distribution. The actin cytoskeleton is depicted in gray levels on a yellow background. Bars = 50 μ m.

Rosenblatt et al., 1997; Moriyama and Yahara, 1999). The similar patterns of actin organization in the *ADF1* knockdown and the *ADF2* knockdown mutant plants suggest that these two ubiquitously expressed AtADF proteins from subclass I perform similar roles.

Analysis of the *ADF2* knockdown plants shows a mild phenotype in hypocotyls and roots, demonstrating that function of *ADF2* in these tissues is redundant. However, reduction in *ADF2* did cause some cell death as evidenced by the lesions on the leaves. Also, in contrast with mutants in other *ADF* genes, knockdown of *ADF2* caused severe defects in reproduction. Siliques were reduced in size and deformed in shape due to underlying defects in embryogenesis and seed development.

As the expression of *ADF2* is upregulated upon infection, we asked whether knockdown of *ADF2* had any effect on actin reorganization in nematode-induced giant cell production and subsequent nematode development. The results presented in this article confirm our previously published observations on the reorganization of actin into thick actin cables at the cortex of

expanding giant cells and the presence of thinner endoplasmic bundles (de Almeida Engler et al., 2004). These actin bundles were randomly distributed between an amorphous fluorescent labeling in the cytoplasm of giant cells. This fluorescence most likely resulted from an excess of newly synthesized monomers or partial depolymerization of the existing filaments (de Almeida Engler et al., 2004). Here, we show that decreased *ADF2* levels stabilize the actin network in giant cells, resulting in the arrest of giant cell development and the cessation of nematode development. However, in plants with decreased levels of *ADF2*, nematodes were able to penetrate, migrate into, and induce gall formation in roots with reduced sizes. However, the giant cells that formed were small, filled with thick bundles of actin, and often arrested at the binucleate stage, and these cells were not able to support nematode development. Moreover, the neighboring cells derived from the vascular parenchyma proliferated abnormally, resulting in the formation of smaller galls. Mutation of ADF/cofilin in various plant species has been shown to arrest cell proliferation and disorganize the actin network (Chen et al.,

2002). Burgos-Rivera et al. (2008) showed that cell proliferation in *Arabidopsis* callus is dependent on ADF9, while Passarinho et al. (2008) demonstrated that *Arabidopsis* ADF9 is upregulated by the activity of a transcription factor (Babyboom) that is important for somatic embryogenesis. Therefore, inhibition of gall expansion in ADF2 knockdown plants is likely due to the reduction of cell proliferation during feeding site formation.

The overall effect of ADF2 knockdown on the actin network of giant cells is most likely caused by a decrease in F-actin turnover, leading to the stabilization and bundling of the actin cytoskeleton. Consequently, nematodes fail to mature into females and produce eggs. These data are supported by our previous observations using the cytoskeleton inhibitors taxol and cytochalasin D (de Almeida Engler et al., 2004). Taxol treatment on infected seedlings induces stabilization of the microtubule cytoskeleton and therefore arrests gall development and nematode maturation. Cytochalasin D (0.5 μ M) treatment induces partial depolymerization of actin filaments in galls and does not impact the numbers of mature females with fertile eggs. Dynamic actin and microtubule cytoskeletons are essential for nematode reproduction. Previous work on the pharmacological interference of the host actin cytoskeleton showed that less organized/more dynamic F-actin may stimulate the internalization of intracellularly acting microbes, contributing to the suppression of antimicrobial defense mechanisms and affecting basal resistance (Kobayashi et al., 1997a, 1997b; Yun et al., 2003; Shimada et al., 2006). Miklis et al. (2007) recently reported that ectopic barley (*Hordeum vulgare*) ADF3 expression compromises actin cytoskeleton integrity and function in barley epidermal cells. They also observed that interference with actin cytoskeleton function is not restricted to a particular ADF isoform but seems to be a general feature of ectopic ADF expression.

It is known that the cytoskeleton is involved in host as well as nonhost resistance (Miklis et al., 2007) and that the plant cytoskeleton behaves differently depending on the plant host and the infecting pathogen. Actin microfilaments are consistently observed to focus on the fungal and oomycete infection sites, and treatments with cytochalasins (inhibitors of actin polymerization) have shown to suppress or delay resistance reactions, such as hypersensitive cell death. Our findings and recently published data on the significance of *Arabidopsis* ADF4 for the regulation of the actin cytoskeleton reorganization required for AvrPphB-mediated resistance against the phytopathogenic bacterium *Pseudomonas syringae* (Tian et al., 2009) suggest that ADF is a key regulator of actin polymerization and organization during plant host/parasite interactions. By contrast, the microtubule response to pathogen attack is much more variable between different plant-microbe interactions (Takemoto and Hardham, 2004). In parsley (*Petroselinum crispum*) or soybean (*Glycine max*) infected by the oomycete *Phytophthora sojae*, localized microtubule depolymerization has been observed (Gross et al., 1993; Cahill et al., 2002). The role of microtubule dynamic regulators during host/parasite interactions is not well understood. In the case of nematode infection, the microtubule network undergoes reorganization and possibly partial depolymerization, and its chemical stabilization by taxol arrests gall development, whereas breakdown allows nematode development (de Almeida Engler et al., 2004). However, so far it has only

been shown that the microtubule bundling protein *Arabidopsis* Microtubule Associated Protein65-3 is required for the ontogenesis of giant cells at the feeding site (Caillaud et al., 2008).

The results presented in this study are in agreement with previous findings that the architecture of the actin cytoskeleton is essential for feeding site development (de Almeida Engler et al., 2004). We have shown that actin reorganization mediated by proteins that modulate actin dynamics is essential for a successful nematode infection of *Arabidopsis*. Expression of ADF2 after infection is a key part of the infection process. This is shown by its early expression and upregulation between 14 and 21 DAI and the effect of its downregulation in causing giant cell and nematode development to fail. We propose that knockdown of ADF2 causes the stabilization of the actin cytoskeleton, which in turn prevents normal giant cell maturation. We suggest that a dynamic actin cytoskeleton is important for giant cell growth and expansion. In addition, we cannot exclude the possibility that the increased amount of F-actin in ADF2 knockdown plants causes an increase in the density of the giant cell cytoplasm, which could hamper the suction and ingestion of its contents during the feeding of the nematodes, thereby halting their life cycle.

METHODS

Constructs and Plant Transformation

Full-length ADF2 was amplified using a forward primer with Gateway (Invitrogen) attB1 and a reverse primer with attB2 sequences. The reverse primer contained BamHI and HindIII restriction sites between the gene-specific sequence and the attB2 sequence. In addition, full-length ADF2 was amplified using a forward primer with a HindIII restriction site 5' of the ADF coding sequence and a reverse primer with a BamHI restriction site 3' of the ADF coding sequence. This fragment was cloned into pGEM-T Easy. Both plasmids were digested with HindIII and BamHI, whereafter *Arabidopsis* ADF2 from pGEM-T Easy was reversely cloned into pDONR207 containing the forward ADF2 so that a subsequent sense and antisense copy of ADF2 was present. The sense-antisense ADF2 fragment was transferred to 35S_{pro}:alcR-RFA (Ketelaar et al., 2007) by a Gateway LR reaction. The resulting 35S_{pro}:alcR-ADF2-RNAi plasmid was transformed into *Agrobacterium tumefaciens* strain C58C1, and *Arabidopsis thaliana* Col-0 plants were transformed by floral dipping (Clough and Bent, 1998).

Plant Material, Growth Conditions, and Nematode Infections

ADF2-RNAi plants were selected from the kanamycin-positive seeds based on their phenotype after ethanol induction, and T2 seed was used throughout. *Arabidopsis* T3 seeds harboring 35S_{pro}:GFP:FABD were used for crossing to ADF2-RNAi lines. Seeds were potted in general purpose compost and sand (4:1) and grown in a growth room (16 h light and 8 h darkness). Three weeks after sowing, the ADF2-RNAi plants that were watered with 25 mL of 0.5% ethanol twice weekly were recorded for phenotype. Surface-sterilized seeds of *Arabidopsis* cv Col-0 and a transgenic line harboring the ethanol-inducible ADF2-RNAi construct were germinated, induced with weekly applications of 0.25% ethanol, and infected as described by de Almeida Engler et al. (1999). Transgenic lines were germinated in 50 mg/mL kanamycin. Seedlings were grown vertically, to allow roots to grow at the surface (facilitating nematode infection), with a 16-h-light/8-h-dark photoperiod at 21°C/18°C, respectively. Resistance was scored, and seedlings were harvested 15 d after germination. Galls of roots infected with 100 surface-sterilized freshly

hatched *Meloidogyne incognita* J2 larvae were harvested 7, 14, and 21 DAI. Samples were immediately frozen in liquid nitrogen for molecular analysis or embedded for microscopy analyses. The *ADF2*-RNAi plants were induced by addition of 0.2% ethanol to the medium 3 d before inoculation, and 0.1% ethanol was added weekly.

Quantitative RT-PCR

RNA of 15-d-old whole ethanol-induced and noninduced *ADF2*-RNAi seedlings was isolated using the RNeasy plant mini kit (Qiagen) to confirm the specific downregulation of *ADF2* in the ethanol-inducible *ADF2*-RNAi line. To analyze the expression levels of seven *ADF* isoforms after nematode infection, 14-d-old seedlings were treated with 0.2% ethanol and 48 h later infected with *M. incognita*. Once a week, 0.2% (25 μ L) of ethanol was added to the medium. RNA were isolated from dissected galls 7, 14, and 21 DAI and nonmeristematic root fragments, without apical and lateral root meristems, from noninfected Col-0 plants as a control. The RNA was treated with RQ1 RNase-free DNase (Promega) before reverse transcription. One microgram of treated RNA was added to RT reactions using a Bio-Rad iScript first-strand synthesis kit with random hexamer primers to make cDNA. Quantitative RT-PCR was performed on a Chromo4 real-time PCR detection system CFB-3240 (Bio-Rad) using SYBR Green detection chemistry. The $2^{-\Delta\Delta Ct}$ method (Livak and Schmittgen, 2001) of relative quantification was used in all experiments. *Ubiquitin-specific protease 22 (UBP22)* expression was used to normalize the transcript levels for each sample. The relative *ADF* gene expression values in 15-d-old whole *ADF2*-RNAi seedlings were calculated as $2^{-\Delta\Delta Ct}$ gene of interest (Ct ethanol noninduced – Ct ethanol induced)/ ΔCt reference gene (Ct ethanol noninduced – Ct ethanol induced), where the gene of interest is one of the *Arabidopsis ADF* genes (*ADF1-6*, *ADF8*, or *ADF10*) and the reference gene is *UBP22*. The *ADF2*-RNAi line is ethanol inducible, and the noninduced *ADF2*-RNAi line was used as the control. The relative *ADF* gene expression values in the dissected galls 7, 14, and 21 DAI infected with *M. incognita* were calculated as $2^{-\Delta\Delta Ct}$ gene of interest (Ct uninfected – Ct infected)/ ΔCt reference gene (Ct uninfected – Ct infected), where the gene of interest is each of the *Arabidopsis ADF* genes (*ADF1-6* or *ADF8*) analyzed, and the reference gene was *UBP22*. Primer sequences for each real-time reaction are listed in Supplemental Table 1 online. Two biological replicates were performed. Three independent quantitative RT-PCR reactions were performed per sample. The bars represent mean values from two independent experiments. Statistically significant differences for values were determined by Wilcoxon test as described by Yuan et al. (2006).

Morphological Analysis

For morphological analysis, uninfected and nematode-infected roots were fixed in 2% glutaraldehyde in 50 mM PIPES buffer, pH 6.9, and then dehydrated and embedded in Technovit 7100 (Heraeus Kulzer) as described by the manufacturer. Embedded tissues were sectioned (3 μ m) and stained in 0.05% toluidine blue and mounted in Depex (Sigma-Aldrich), and microscopy was performed using bright-field optics. For nuclei counting, serial sections stained with toluidine blue were examined using bright-field optics or stained with 4',6-diamidino-2-phenylindole (1 μ g/mL) in PIPES buffer and analyzed by epifluorescence microscopy. Images were collected with a digital camera (Axiocam; Zeiss).

Histochemical GUS Assay and Microscopy Analysis

Transgenic plants carrying five different constructs containing translational fusions of *ADF_{pro}:GUS* (Ruzicka et al., 2007) were kind gifts of Richard Meagher (Department of Genetics, University of Georgia). Expression patterns of *Arabidopsis ADF2*, *ADF3*, *ADF4*, *ADF6*, and *ADF10* lines were monitored at different time points after nematode infection (7, 14, and 21 DAI) as previously described (de Almeida Engler et al., 1999). To avoid diffusion of the GUS, stained galls were fixed in 2.0% glutar-

aldehyde and were embedded in Technovit 7100, sectioned, and microscopically analyzed by dark-field optics. Otherwise, seedlings were fixed and transferred to the chloralactophenol-clearing solution (Beeckman and Engler, 1994) for observation by Normasky optics.

Immunocytochemistry

Nematode-infected roots and uninfected roots of *Arabidopsis* cv Col-0 were fixed in 4% formaldehyde in 50 mM PIPES buffer, pH 6.9. Feeding sites and uninfected roots were dehydrated and embedded in butyl-methylmethacrylate as described by Kronenberger et al. (1993). Sectioned material (5 μ m) was treated with acetone for 30 min to remove the embedding medium. Primary and secondary antibodies were diluted 100- and 300-fold, respectively, in blocking solution (1% BSA in 50 mM PIPES buffer, pH 6.9) and 0.2% DMSO. Sections were incubated with blocking solution for 30 min and then overnight at 4°C with the following primary antibody: polyclonal rabbit anti-ZmADF3 (Jiang et al., 1997). As control, primary antibody was omitted in some slides. Slides were washed twice for 15 min each in PIPES buffer. A 2-h incubation at room temperature was performed with the following secondary antibody: Alexa 488 goat anti-rabbit IgG (Molecular Probes) to visualize ADF. Slides were washed for 30 min in PIPES buffer. Slides were mounted in 90% glycerol and imaged for ADF. Subsequently, slides were incubated overnight at 4°C with the second primary antibody: monoclonal mouse anti-ACT clone 4 (ICN). Slides were washed twice for 15 min each in PIPES buffer. A 2-h incubation at 37°C was performed with the following secondary antibody: Alexa 594 goat antimouse IgG to visualize ACTs. DNA was stained with 1 μ g mL⁻¹ 4',6-diamidino-2-phenylindole (Sigma-Aldrich) in PIPES buffer and briefly rinsed twice in deionized water to remove salt. Slides were mounted in ProLong Antifade Kit (Molecular Probes). Samples were observed with a microscope (Axioskop; Zeiss) equipped for epifluorescence microscopy, and images were acquired with a digital camera (Axiocam; Zeiss).

LatB Treatment

Leaves of induced *ADF2*-RNAi and control plants, both expressing the actin marker GFP:FABD (Ketelaar et al., 2004), were treated with 5 μ M LatB for 1 h. Images of LatB-treated and untreated leaf cells were taken of induced and noninduced *ADF2*-RNAi plants grown in soil. Leaves were incubated in water with or without 5 μ M LatB, and Z-stacks were collected on a Zeiss LSM510 META, mounted to a Zeiss Axiovert 200 stand with a Zeiss $\times 63$ α -Plan-Fluar oil immersion objective (numerical aperture 1.4), using 3 to 5% of the 488-nm laser line and the 488/543 dichroic mirror and the BP505-530 emission filter. Z-stacks were projected using the maximum projection function of the Zeiss LSM image examiner (version 3.5.0.223) software package.

Nematode Infection Test

Seedlings of *ADF2*-RNAi induced with ethanol, noninduced *Arabidopsis* cv Col-0, and ecotype Wassilewskija were infected in vitro 14 d after germination with 100 surface-sterilized freshly hatched *M. incognita* J2. *Arabidopsis* cv Col-0 and Wassilewskija were used as controls to find out if ethanol treatment might affect nematode viability. Infected seedlings were kept at 20°C with a 16-h photoperiod. Best results for *ADF_{pro}:GUS* expression, without affecting the seedlings, were obtained by adding 0.2% (25 μ L) of ethanol weekly to the medium. During infection tests, egg mass counting was performed 60 DAI to allow nematodes to complete their life cycle.

Confocal Microscopy

To visualize the actin cytoskeleton of seedlings and nematode feeding sites, chimeric *ADF2*-RNAi ethanol-induced and noninduced seedlings

harboring a GFP fused to FABD under the control of the 35S promoter were analyzed and compared. Based on fluorescence of the thinnest bundle, actin bundle thickness present within the different cell types (i.e., leaf mesophyll and root vascular tissues) was measured.

For *in vivo* observations, nematode-infected and uninfected sterile transgenic seedlings were transferred to a Chambered Coverglass System (Lab-Tek) and covered with KNOP medium for observation. Whole infected and uninfected seedlings were analyzed on a confocal microscope (model LSM510 META; Zeiss). To obtain a three-dimensional view, 30 to 50 optical sections collected at different focal planes, at intervals of 1.5 μm , were used to generate projections. To allow visualization of the actin cytoskeleton in giant cells (7 to 14 DA), laying deep within the root vascular tissue, galls were dissected and embedded in 5% agarose. To eliminate the cell layers covering the feeding site, vibraslices of 150 to 200 μm were obtained using a vibratome HM560V (Microm). Shadow three-dimensional view projections were generated using the Carl Zeiss ZEN 2007 software.

Accession Numbers

Sequence data from this article can be found in the Arabidopsis Genome Initiative or GenBank/EMBL databases under the following accession numbers: At *ADF1*, NM_114470 (At3g46010); At *ADF2*, NM_114469 (At3g46000); At *ADF3*, NM_125381 (At5g59880); At *ADF4*, NM_125382 (At5g59890); At *ADF5*, NM_127222 (At2g16700); At *ADF6*, NM_128676 (At2g31200); At *ADF8*, NM_116293 (At4g00680); and At *ADF10*, NM_124615 (At5g52360). The Arabidopsis Genome Initiative locus numbers are given in parenthesis.

Supplemental Data

The following materials are available in the online version of this article.

Supplemental Figure 1. Anti-*Z. mays* ADF3 Cross-React with Several *Arabidopsis* ADF Isoforms.

Supplemental Figure 2. Morphological Analysis of the Shoot Apex of *ADF2* Knockdown Line and Noninduced Control Seedlings.

Supplemental Table 1. Primer Sequences Used in qRT-PCR Amplification of the Eight ADF Gene Transcripts.

ACKNOWLEDGMENTS

We thank Richard B. Meagher and Muthugapatti K. Kandasamy from the University of Georgia for kindly providing the five different constructs containing translational fusions of *ADF_{pro}*:GUS (*ADF2*, *ADF3*, *ADF4*, *ADF6*, and *ADF10* lines).

Received June 3, 2009; revised August 14, 2009; accepted September 1, 2009; published September 30, 2009.

REFERENCES

- Allwood, E.G., Anthony, R.G., Smertenko, A.P., Reichelt, S., Drodak, B.K., Doonan, J.H., Weeds, A.G., and Hussey, P.J. (2002). Regulation of the pollen-specific actin-depolymerizing factor LIADF1. *Plant Cell* **14**: 2915–2927.
- Andrianantoandro, E., and Pollard, T.D. (2006). Mechanism of actin filament turnover by severing and nucleation at different concentrations of ADF/cofilin. *Mol. Cell* **24**: 13–23.
- Augustine, R.C., Vidali, L., Kleinman, K.P., and Bezanilla, M. (2008). Actin depolymerizing factor is essential for viability in plants, and its phosphoregulation is important for tip growth. *Plant J.* **54**: 863–875.
- Ayscough, K.R. (1998). *In vivo* functions of actin-binding proteins. *Curr. Opin. Cell Biol.* **10**: 102–111.
- Ayscough, K.R., Stryker, J., Pokala, N., Sanders, M., Crews, P., and Drubin, D.G. (1997). High rates of actin filament turnover in budding yeast and roles for actin in establishment and maintenance of cell polarity revealed using the actin inhibitor Latrunculin-A. *J. Cell Biol.* **137**: 399–416.
- Bamburg, J.R. (1999). Proteins of the ADF/cofilin family: Essential regulators of actin dynamics. *Annu. Rev. Cell Dev. Biol.* **15**: 185–230.
- Beeckman, T., and Engler, G. (1994). An easy technique for the clearing of histochemically stained plant tissue. *Plant Mol. Biol. Rep.* **12**: 37–42.
- Bettinger, B.T., Gilbert, D.M., and Amberg, D.C. (2004). Actin up in the nucleus. *Nat. Rev. Mol. Cell Biol.* **5**: 410–415.
- Bird, A.F. (1971). Quantitative studies on the growth of syncytia induced in plants by root knot nematodes. *Int. J. Parasitol.* **2**: 157–170.
- Bird, D.M., and Kaloshian, I. (2003). Are roots special? Nematodes have their say. *Physiol. Mol. Plant Pathol.* **62**: 115–123.
- Burgos-Rivera, B., Ruzicka, D.R., Deal, R.B., McKinney, E.C., King-Reid, L., and Meagher, R.B. (2008). Actin depolymerizing factor9 controls development and gene expression in *Arabidopsis*. *Plant Mol. Biol.* **68**: 619–632.
- Cahill, D., Rookes, J., Michalczyk, A., McDonald, K., and Drake, A. (2002). Microtubule dynamics in compatible and incompatible interactions of soybean hypocotyl cells with *Phytophthora sojae*. *Plant Pathol.* **51**: 629–640.
- Caillaud, M.C., Lecomte, P., Jammes, F., Quentin, M., Pagnotta, S., Andrio, E., de Almeida Engler, J., Marfaing, N., Gounon, P., Abad, P., and Favery, B. (2008). MAP65-3 microtubule-associated protein is essential for nematode-induced giant cell ontogenesis in *Arabidopsis*. *Plant Cell* **20**: 423–437.
- Carlier, M.F. (1998). Control of actin dynamics. *Curr. Opin. Cell Biol.* **10**: 45–51.
- Carlier, M.F., Laurent, V., Santolini, J., Melki, R., Didry, D., Xia, G.X., Hong, Y., Chua, N.H., and Pantaloni, D. (1997). Actin depolymerizing factor (ADF/cofilin) enhances the rate of filament turnover: Implication in actin-based motility. *J. Cell Biol.* **136**: 1307–1322.
- Chen, C.Y., Wong, E.I., Vidali, L., Estavillo, A., Hepler, P.K., Wu, H. M., and Cheung, A.Y. (2002). The regulation of actin organization by actin-depolymerizing factor in elongating pollen tubes. *Plant Cell* **14**: 2175–2190.
- Chen, H., Bernstein, B.W., and Bamburg, J.R. (2000). Regulating actin filament dynamics *in vivo*. *Trends Biochem. Sci.* **25**: 19–23.
- Clough, S.J., and Bent, A.F. (1998). Floral dip: A simplified method for Agrobacterium-mediated transformation of *Arabidopsis thaliana*. *Plant J.* **16**: 735–743.
- de Almeida Engler, J., De Vleeschauwer, V., Bursens, S., Celenza, J.L., Jr., Inzé, D., Van Montagu, M., Engler, G., and Gheysen, G. (1999). Molecular markers and cell cycle inhibitors show the importance of cell cycle progression in nematode-induced galls and syncytia. *Plant Cell* **11**: 793–808.
- de Almeida Engler, J., Favery, B., Engler, G., and Abad, P. (2005). Loss of susceptibility as an alternative for nematode resistance. *Curr. Opin. Biotechnol.* **16**: 112–117.
- de Almeida Engler, J., Van Poucke, K., Karimi, M., De Groodt, R., Gheysen, G., and Engler, G. (2004). Dynamic cytoskeleton rearrangements in giant cells and syncytia of nematode-infected roots. *Plant J.* **38**: 12–26.
- Dong, C.H., Kost, B., Xia, G.X., and Chua, N.H. (2001a). Molecular identification and characterization of *AtADF1*, *AtADF5*, and *AtADF6* genes. *Plant Mol. Biol.* **45**: 517–527.

- Dong, C.H., Xia, G.X., Hong, Y., Ramachandran, S., Kost, B., and Chua, N.H.** (2001b). ADF proteins are involved in the control of flowering and regulate F-actin organization, cell expansion, and organ growth in *Arabidopsis*. *Plant Cell* **13**: 1333–1346.
- Favery, B., Chelysheva, L.A., Lebris, M., Jammes, F., Marmagne, A., De Almeida Engler, J., Lecomte, P., Vaury, C., Arkowitz, R.A., and Abad, P.** (2004). *Arabidopsis* formin AtFH6 is a plasma membrane-associated protein upregulated in giant cells induced by parasitic nematodes. *Plant Cell* **16**: 2529–2540.
- Feng, Y., Liu, Q., and Xue, Q.** (2006). Comparative study of rice and *Arabidopsis* actin-depolymerizing factors gene families. *J. Plant Physiol.* **163**: 69–79.
- Fuller, V.L., Lilley, C.J., Atkinson, H.J., and Urwin, P.** (2007). Differential gene expression in *Arabidopsis* following infection by plant-parasitic nematodes *Meloidogyne incognita* and *Heterodera schachtii*. *Mol. Plant Pathol.* **8**: 595–609.
- Fuller, V.L., Lilley, C.J., and Urwin, P.E.** (2008). Nematode resistance. *New Phytol.* **180**: 27–44.
- Gross, P., Julius, C., Schmelzer, E., and Hahlbrock, K.** (1993). Translocation of cytoplasm and nucleus to fungal penetration sites is associated with depolymerization of microtubules and defence gene activation in infected, cultured parsley cells. *EMBO J.* **12**: 1735–1744.
- Hussey, P.J., Ketelaar, T., and Deeks, M.J.** (2006). Control of the actin cytoskeleton in plant cell growth. *Annu. Rev. Plant Biol.* **57**: 109–125.
- Jammes, F., Lecomte, P., de Almeida Engler, J., Bitton, F., Martin-Magniette, M.L., Renou, J.P., Abad, P., and Favery, B.** (2005). Genome-wide expression profiling of the host response to root-knot nematode infection in *Arabidopsis*. *Plant J.* **44**: 447–458.
- Jiang, C.J., Weeds, A.G., and Hussey, P.J.** (1997). The maize actin-depolymerizing factor, ZmADF3, redistributes to the growing tip of elongating root hairs and can be induced to translocate into the nucleus with actin. *Plant J.* **12**: 1035–1043.
- Jones, M.G.K., and Northcote, D.H.** (1972). Nematode-induced syncytium - A multinucleate transfer cell. *J. Cell Sci.* **10**: 789–809.
- Kandasamy, M.K., Burgos-Rivera, B., McKinney, E.C., Ruzicka, D. R., and Meagher, R.B.** (2007). Class-specific interaction of profilin and ADF isoforms with actin in the regulation of plant development. *Plant Cell* **19**: 3111–3126.
- Ketelaar, T., Allwood, E.G., Anthony, R., Voigt, B., Menzel, D., and Hussey, P.J.** (2004). The actin-interacting protein AIP1 is essential for actin organization and plant development. *Curr. Biol.* **14**: 145–149.
- Ketelaar, T., Allwood, E.G., and Hussey, P.J.** (2007). Actin organization and root hair development are disrupted by ethanol-induced overexpression of *Arabidopsis* actin interacting protein 1 (AIP1). *New Phytol.* **174**: 57–62.
- Kim, S.R., Kim, Y., and An, G.** (1993). Molecular cloning and characterization of anther-preferential cDNA encoding a putative actin-depolymerizing factor. *Plant Mol. Biol.* **21**: 39–45.
- Kobayashi, I., Kobayashi, Y., and Hardham, A.R.** (1997a). Inhibition of rust-induced hypersensitive response in flax cells by the microtubule inhibitor oryzalin. *Aust. J. Plant Physiol.* **24**: 733–740.
- Kobayashi, Y., Kobayashi, I., Funaki, Y., Fujimoto, S., Takemoto, T., and Kunoh, H.** (1997b). Dynamic reorganization of microfilaments and microtubules is necessary for the expression of non-host resistance in barley coleoptile cells. *Plant J.* **11**: 525–537.
- Kost, B., Mathur, J., and Chua, N.J.** (1999). Cytoskeleton in plant development. *Curr. Opin. Plant Biol.* **2**: 462–470.
- Kronenberg, J., Desprez, T., Höfte, H., Caboche, M., and Traas, J.** (1993). A methacrylate embedding procedure developed for immunolocalization on plant tissues is also compatible with *in situ* hybridization. *Cell Biol. Int.* **17**: 1013–1021.
- Lappalainen, P., and Drubin, D.G.** (1997). Cofilin promotes rapid actin filament turnover in vivo. *Nature* **388**: 78–82.
- Livak, K.J., and Schmittgen, T.D.** (2001). Analysis of relative gene expression data using real-time quantitative PCR and the 2(-Delta Delta C(T)) method. *Methods* **25**: 402–408.
- Lopez, I., Anthony, R.G., Maciver, S.K., Jiang, C.J., Khan, S., Weeds, A., and Hussey, P.J.** (1996). Pollen specific expression of maize genes encoding actin depolymerizing factor-like proteins. *Proc. Natl. Acad. Sci. USA* **93**: 7415–7420.
- Mabuchi, I.** (1983). An actin-depolymerizing protein (depactin) from starfish oocytes: properties and interaction with actin. *J. Cell Biol.* **97**: 1612–1621.
- Maciver, S.K.** (1998). How ADF/cofilin depolymerizes actin filaments. *Curr. Opin. Cell Biol.* **10**: 140–144.
- Maciver, S.K., and Hussey, P.J.** (2002). The ADF/cofilin family: Actin-remodeling proteins. *Genome Biol.* **3**: reviews 3007.1–3007.12.
- Maciver, S.K., Zot, H.G., and Pollard, T.D.** (1991). Characterization of actin filament severing by actophorin from *Acanthamoeba castellanii*. *J. Cell Biol.* **115**: 1611–1620.
- McGough, A., Pope, B., and Weeds, A.** (2001). The ADF/Cofilin family: Accelerators of actin reorganization. *Results Probl. Cell Differ.* **32**: 135–154.
- Meagher, R.B., McKinney, E.C., and Kandasamy, M.K.** (1999). Isovariant dynamics expand and buffer the responses of complex systems: The diverse plant actin gene family. *Plant Cell* **11**: 995–1005.
- Miklis, M., Consonni, C., Bhat, R.A., Lipka, V., Schulze-Lefert, P., and Panstruga, R.** (2007). Barley MLO modulates actin-dependent and actin-independent antifungal defense pathways at the cell periphery. *Plant Physiol.* **144**: 1132–1143.
- Minakhina, S., Myers, R., Druzhinina, M., and Steward, R.** (2005). Crosstalk between the actin cytoskeleton and Ran-mediated nuclear transport. *BMC Cell Biol.* **6**: 32.
- Moriyama, K., and Yahara, I.** (1999). Two activities of cofilin, severing and accelerating directional depolymerization of actin filaments, are affected differentially by mutations around the actin-binding helix. *EMBO J.* **18**: 6752–6761.
- Nishida, E., Iida, K., Yonezawa, N., Koyasu, S., Yahara, I., and Sakai, H.** (1987). Cofilin is a component of intranuclear and cytoplasmic actin rods induced in cultured cells. *Proc. Natl. Acad. Sci. USA* **84**: 5262–5266.
- Passarinho, P., Ketelaar, T., Xing, M., van Arkel, J., Maliepaard, C., Hendriks, M.W., Joosen, R., Lammers, M., Herdies, L., den Boer, B., van der Geest, L., and Boutilier, K.** (2008). BABY BOOM target genes provide diverse entry points into cell proliferation and cell growth pathways. *Plant Mol. Biol.* **68**: 225–237.
- Pavlov, D., Muhrad, A., Cooper, J., Wear, M., and Reisler, E.** (2007). Actin filament severing by cofilin. *J. Mol. Biol.* **365**: 1350–1358.
- Pendleton, A., Pope, B., Weeds, A., and Koffer, A.** (2003). Latrunculin B or ATP depletion induces cofilin-dependent translocation of actin into nuclei of mast cells. *J. Biol. Chem.* **278**: 14394–14400.
- Rhee, S.Y., et al.** (2003). The *Arabidopsis* Information Resource (TAIR): A model organism database providing a centralized, curated gateway to *Arabidopsis* biology, research materials and community. *Nucleic Acids Res.* **31**: 224–228.
- Rosenblatt, J., Agnew, B.J., Abe, H., Bamberg, J.R., and Mitchison, T.J.** (1997). *Xenopus* actin depolymerizing factor/cofilin (XAC) is responsible for the turnover of actin filaments in *Listeria monocytogenes* tails. *J. Cell Biol.* **136**: 1323–1332.
- Ruzicka, D.R., Kandasamy, M.K., McKinney, E.C., Burgos-Rivera, B., and Meagher, R.B.** (2007). The ancient subclasses of *Arabidopsis* actin depolymerizing factor genes exhibit novel and differential expression. *Plant J.* **52**: 460–472.
- Sijmons, P.C., Grundle, F.M.W., von Mende, N., Burrows, P.R., and**

- Wyss, U.** (1991). *Arabidopsis thaliana* as a new model host for plant-parasitic nematodes. *Plant J.* **1**: 245–254.
- Shimada, C., Lipka, V., O'Connell, R., Okuno, T., Schulze-Lefert, P., and Takano, Y.** (2006). Non-host resistance in *Arabidopsis*–Colletotrichum interactions acts at the cell periphery and requires actin filament function. *Mol. Plant Microbe Interact.* **19**: 270–279.
- Smertenko, A.P., Jiang, C.J., Simmons, N.J., Weeds, A.G., Davies, D.R., and Hussey, P.J.** (1998). Ser6 in the maize actin depolymerizing factor, ZmADF3, is phosphorylated by a calcium stimulated protein kinase and is essential for the control of functional activity. *Plant J.* **14**: 187–193.
- Staiger, C.J.** (2000). Signaling to the actin cytoskeleton in plants. *Annu. Rev. Plant Physiol. Plant Mol. Biol.* **51**: 257–288.
- Staiger, C.J., and Blanchoin, L.** (2006). Actin dynamics: Old friends with new stories. *Curr. Opin. Plant Biol.* **9**: 554–562.
- Staiger, C.J., Gibbon, B.C., Kovar, D.R., and Zonia, L.E.** (1997). Profilin and actin-depolymerizing factor: Modulators of actin organization in plants. *Trends Plant Sci.* **2**: 275–281.
- Takemoto, D., and Hardham, A.R.** (2004). The cytoskeleton as a regulator and target of biotic interactions in plants. *Plant Physiol.* **136**: 3864–3876.
- Tian, M., Chaudhry, F., Ruzicka, D.R., Meagher, R.B., Staiger, C.J., and Day, B.** (2009). *Arabidopsis* actin depolymerizing factor AtADF4 mediates defense signal transduction triggered by the *Pseudomonas syringae* effector AvrPphB. *Plant Physiol.* .
- Van Troys, M., Huyck, L., Leyman, S., Dhaese, S., Vandekerckhove, J., and Ampe, C.** (2008). Ins and outs of ADF/cofilin activity and regulation. *Eur. J. Cell Biol.* **87**: 649–667.
- Volkman, D., and Baluska, F.** (1999). Actin cytoskeleton in plants: From transport networks to signaling networks. *Microsc. Res. Tech.* **47**: 135–154.
- Wasteneys, G.O., and Galway, M.E.** (2003). Remodeling the cytoskeleton for growth and form: An overview with some new views. *Annu. Rev. Plant Biol.* **54**: 691–722.
- Yormola, E.G., Somasundaram, T., Boring, T.A., Spector, I., and Bubb, M.R.** (2000). Actin-latrunculin A structure and function: Differential modulation of actin-binding protein function by latrunculin A. *J. Biol. Chem.* **275**: 28120–28127.
- Yuan, S.J., Reed, A., Chen, F., and Neal Stewart Jr, C.** (2006). Statistical analysis of real-time PCR data. *BMC Bioinformatics* **7**: 85–97.
- Yun, B.-W., Atkinson, H.A., Gaborit, C., Greenland, A., Read, N.D., Pallas, J.A., and Loake, G.J.** (2003). Loss of actin cytoskeletal function and EDS1 activity, in combination, severely compromises non-host resistance in *Arabidopsis* against wheat powdery mildew. *Plant J.* **34**: 768–777.